2022

Design Of A Two-phase Reciprocating Expansion Test-rig For Model Validation

Xander van Heule

Elias Vieren

Michel De Paepe

Steven Lecompte

Design of a two-phase reciprocating expansion test-rig for model validation

Xander VAN HEULE[1]*, Elias VIEREN[1], Michel DE PAEPE[1], Steven LECOMPTE[1]

[1]Ghent University, Department of Electromechanical, systems and Metal Engineering, Ghent, Belgium, Sint-Pietersnieuwstraat 41, 9000

Contact Information: Xander.vanheule@ugent.be
* Corresponding Author

ABSTRACT

Two-phase expansion processes have gathered increased interest over the past years. Possible applications are found in conversion of low-grade heat to power, ranging from solar and geothermal heat to automotive and industrial waste heat. Currently, these applications make use of the basic Organic Rankine Cycle (ORC) concept. However, theoretical studies of two-phase cycles, such as the Trilateral cycle (TLC) and the Partial Evaporation Organic Rankine Cycle (PEORC), show efficiency improvements of over 15% compared to the basic ORC. Two-phase expansion is also beneficial in heat pumps. Substituting the classical throttle valve with a two-phase expansion device allows a COP increase by 7 to 10%. Yet, the fundamentals of two-phase liquid-vapor expansion are not fully understood. Hence, there are no effective guidelines to design two-phase expanders. During the rapid expansion in the two-phase region, the two-phase mixture goes through various thermodynamic non-equilibrium states. These non-equilibrium states are marked by a mixture consisting of saturated vapor and superheated liquid at saturation pressure. This makes the actual prediction of the flashing evaporation rate challenging. In previous work by the authors, the evaporation rate of the mixture was predicted by a Homogeneous Relaxation Model (HRM). In this study, an experimental test rig is presented which is capable to expand two-phase refrigerants in representative working conditions. The goal is to measure the pressure and temperature profiles during expansion. With this unique dataset, the predictive model will be calibrated and validated in future work.

1. INTRODUCTION

Presently, climate change is an international problem. Resulting in sea level rise, declining arctic ice, ocean acidification, and more extreme weather events. The cause is primarily human activity, mostly due to the burning of fossil fuels which increases the concentration of greenhouse gases in the atmosphere (Bailey *et al.*, 2022). Therefore, research is done to decrease the human impact and/or to counteract the effects. A part of the solution is to further increase energy efficiency. The global overall end-use efficiency of primary fuel is around 28%. The majority (52%) of the remainder is found in residual heat of exhausts and effluents (Forman *et al.*, 2016). This heat is available in a wide range of temperatures, from temperatures greater than 300°C to temperatures below 100°C. The Organic Rankine Cycle can effectively convert these low grade heat streams to power (Lecompte *et al.*, 2015a).

For these low-temperature sources, the performance of a basic ORC reduces drastically (Branchini *et al.*, 2013). Part of this has to do with the increased relevance of the temperature mismatch between working fluid and heat carrier. Several concepts are formulated to improve this (Lecompte *et al.*, 2015a). The two main cycles of interest here are the trilateral cycle (TLC) and the partial evaporation organic Rankine cycle (PEORC). The main components of these two cycles are similar as for a basic ORC. The difference between the three cycles is represented on Figure 1.

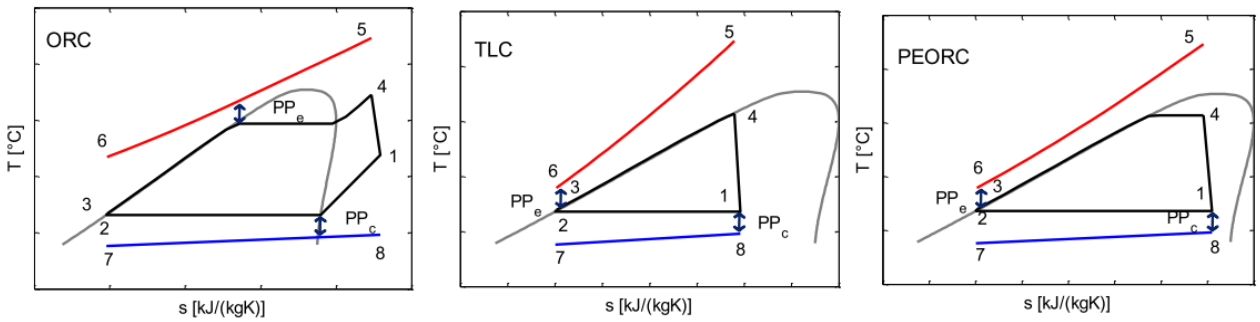

Figure 1: T-s diagrams of the basic ORC, TLC, and PEORC (Lecompte *et al.*, 2015b).

The difference between the three cycles is the state at the entrance of the expander. In the basic ORC this is typically a superheated vapor as shown on the first plot of Figure 1. The TLC on the other hand has a saturated liquid at the expander inlet, and the PEORC has an expander intake in the two-phase region. Fischer (2011) compared the TLC with the ORC based on case studies. The author concluded that the exergy efficiency for power production, which is the ratio of the net power output to the incoming exergy flow of the heat carrier, is 14 to 29% higher for the TLC than for the ORC. Li *et al.* (2017) also compared the cycles based on thermodynamic models. The authors also concluded that the TLC performs better thermodynamically. However, both authors mention the extra requirements on the evaporator and the flow rate due to the fact that the evaporator no longer benefits from the boiling heat transfer. Therefore, a larger flow rate is required for the same exchanged power and the heat exchanger requires a larger UA value. The PEORC is a compromise between the basic ORC and the TLC, it can be used to still benefit from the latent heat and the boiling heat transfer, thereby reducing the volumetric flow rate and the UA value. The PEORC can also even still improve the net power output of the system compared to the TLC (Lecompte *et al.*, 2013).

Efficient two-phase expanders are thus necessary to effectively use the TLC and PEORC cycles as these expand through the two-phase region, as can be seen by the process from state 4 to state 1 on Figure 1. But these cycles are not the only possible application. For instance, a two-phase expander can be used instead of a throttling valve in heat pumps (Galoppi *et al.*, 2017) or in refrigeration cycles such as the liquefication of natural gas (Qyyum *et al.*, 2018).

1.1 Expander types for low grade heat recovery

The selection of the expansion machine is strongly correlated with operating conditions and system size. Current low grade heat recovery sources are typically smaller in size and thus make use of volumetric expanders (Imran *et al.*, 2016). For basic ORCs four main types of expanders are typically used (Imran *et al.*, 2016): vane expander, scroll expander, piston expander, or a screw expander. Each of these expanders has different benefits and technological maturity. For each application, it is recommended to choose the type of expander in parallel with the selection of ORC architecture, range of power, operating condition, and working fluid (Dumont *et al.*, 2017). For the TLC and PEORC the choice for a volumetric expander is beneficial as well, not only for the reason mentioned above but also because volumetric expanders can inherently deal with two-phase conditions. Currently, only the screw or Lysholm expander (Bianchi *et al.*, 2018) and the piston or reciprocating expander (Wang *et al.*, 2019) are found in research in context of two-phase expansion. The benefit of the Lysholm expander is that the assumption of thermodynamic equilibrium gives rather accurate results with experiments (Vasuthevan and Brümmer, 2016). This is likely due to the mixing within the working chambers (Taniguchi *et al.*, 1988). This equilibrium assumption cannot simply be applied to piston expanders as this leads to big discrepancies with experiments (Kanno and Shikazono, 2015). The major benefits of the piston expander are its build-in volume ratio (BVR) which is the largest of all volumetric expanders and its rather simple working chamber shape. For these reasons, the piston expander is chosen to experimentally measure the two-phase expansion vapor generation rate.

1.2 Two-phase flashing

The expansion stroke in a reciprocating expander is described as a two-phase flashing phenomenon. Flashing is a rapid depressurization process that causes a liquid to be in a metastable superheated state. In volumetric expanders, this is a result of the increase in working chamber volume. There exist a plethora of models to describe the flashing phenomenon (Liao and Lucas, 2017). For the piston expander, mechanical equilibrium is assumed but thermal equilibrium is not. This implies that the liquid and vapor phases have the same pressure but not the same temperature.

In addition, the vapor is assumed to be in a saturated state while the liquid is in a metastable superheated state. This leaves three models: the mixture model, the boiling delay model, and the homogeneous relaxation model (HRM). The mixture model solves the continuity equations of the phases and of the mixture. This is accurate but requires many equations and a lot of computational power. The boiling delay model states that the boiling happens only with a certain degree of superheat in the liquid, when the nucleation of bubbles starts to take place. The bubble nucleation and growth also limits the eventual vapor generation rate. The HRM consists of the continuity equations of the mixture together with a vapor generation rate equation based on an empirical thermal relaxation time (Θ). Here it was chosen to use the HRM as it describes a complex behavior in a singular way while still achieving good results (Bilicki *et al.*, 1996).

2. DESCRIPTION OF THE EXPERIMENTAL TEST-RIG

The goal is to construct an experimental setup capable of measuring the pressure and temperature profiles of both the vapor and liquid phase throughout the expansion process in a reciprocating expander. Figure 2 gives a schematic overview of the setup. The flow conditioner creates a constant flow at a defined two-phase state which can be controlled. This constant flow goes through the bypass until the required measurement point is stable.

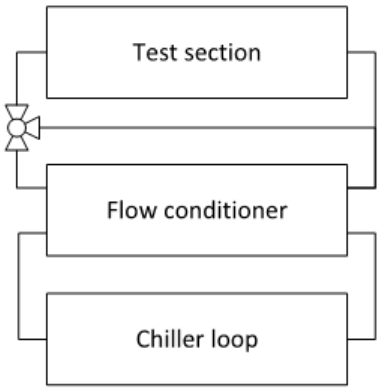

Figure 2: Schematic overview of the test setup. Consisting of three parts: the chiller loop, the flow conditioner, and the test section**.**

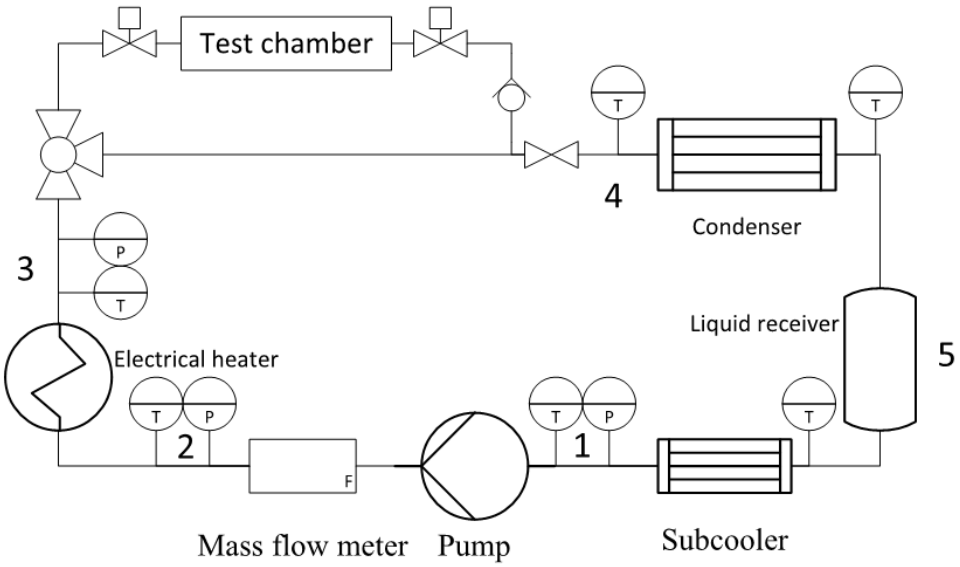

Figure 3: Simplified PID of the flow conditioner.

The conditioned inlet state can then be routed through the piston (i.e. test chamber). When this is achieved the filled piston can be isolated and the continuous flow is again routed through the bypass. The isolated volume in the piston is now ready for the experiment. After the measurement, the exhaust of the piston is connected to the end of the bypass. The simplified flow conditioner with test chamber is shown in Figure 3. Here some less-crucial parts are omitted such as overpressure safety valves.

The condenser and subcooler on Figure 3 make use of the chiller loop as secondary flow. The thermodynamic state required as initial point for an expansion test should be conditioned in point 3 on Figure 3. This can be achieved by changing the settings of the pump, electrical heater, pressure-reducing valve, and chiller loop. The quality of state 3 can be calculated through the energy conservation over the electrical heater. In state 3 the pressure and temperature are measured for two reasons. Firstly as a control, both measurements should indicate the corresponding saturation value. The second reason is for validating the measurements coming from the setup. Two parts will be validated by performing the experimental procedure on superheated vapor expansion tests. Firstly, the processes of expansion with superheated vapor in a reciprocating expander are well known. With the inlet state known due to the pressure and temperature measurements in state 3, the expansion chamber can be validated. Secondly, the methodology of determining the vapor quality by added electrical power can also be validated by performing the same calculations from subcooled liquid to superheated vapor, where the added electrical specific power should correspond to the added fluid enthalpy.

The test chamber on Figure 3 is a reciprocating expander that is controlled with a linear actuator. The actuator can impose a multitude of different movement profiles, and is able to change the BVR of the piston. This can be achieved by starting with a bigger dead volume or not using the entire stroke of the piston. The test section allows for an easy interchange of test chambers. As such it is possible to test different bores as well.

3. SIZING MODEL

As mentioned, the sizing of the first test chamber was performed by modeling of the expansion process. Because the choice was made for a reciprocating expander there is a necessity to describe the thermal instability of the process. The chosen model for this was the HRM, as it is not as computationally demanding while still agreeing with experiments. The HRM consists of the well-known continuity equations supplemented by a vapor mass balance equation. This relaxation equation, in its simplest linear approximation, is given by equation (1) (Downar-Zapolski, 1996):

$$\Gamma_g = \frac{\bar{x} - x}{\Theta} \cdot \rho \tag{1}$$

where Γ_g is the vapor generation rate, x is the current vapor quality, $\bar{x}$ is the equilibrium vapor quality the mixture would tend to if left in the current state , Θ is the thermal relaxation time, and ρ is the density. Downar-Zapolski *et al.*(1996) found that the local relaxation time is a monotonically decreasing function of the void fraction and the non-dimensional pressure difference. The following equations (2,3,4) are applied:

$$\Theta = \Theta_0 \cdot \epsilon^a \cdot \psi^b \tag{2}$$

$$\psi_{<10\text{bar}} = \frac{p_s - p}{p_s} \tag{3}$$

$$\psi_{>10bar} = \frac{p_s - p}{p_c - p_s} \tag{4}$$

where ϵ is the void fraction, ψ is the non-dimensional pressure difference, p_s the saturation pressure at the liquid temperature, p the pressure, and p_c the critical pressure. Θ_0, a, and b are parameters that were also determined by Downar-Zapolski *et al.*(1996) based on the Moby Dick experiments which used water as working fluid. The found values are respectively 6.51×10^{-4} sec, -0.257 and -2.24 for pressures under 10 bar and 3.84×10^{-7} sec, -0.54, and -1.76 for pressures over 10 bar. The definition of ψ is dependent on the pressure, equation 3 is used for pressures under 10 bar and equation 4 for pressures over 10 bar. The values of the three parameters and the pressure limit where the other equations are used are all dependent on the process and the working fluid. However, because no experimental data is available for the examined process, the same values for these parameters are taken for initial simulations.

The simulation model consists of a system of differential equations solved by the numerical LSODA solver. It is based on the work of Lecompte *et al.* (2017) but extended by adding the thermal non-equilibrium model. Because the experiments are solely for the expansion stroke and not the intake stroke, the inlet mass flow rate is omitted. The following equations are the ODE system:

$$\mathrm{m_p} \cdot a = \frac{\pi \cdot D_{cyl}^2}{4} \cdot \left(p_{cyl} - p_{bp}\right) - F_{fr} - F_{load} \tag{5}$$

$$\dot{\mathrm{Q}}_{\mathrm{cyl}} = \mathrm{h_{wall}} \cdot \mathrm{A_{wall}} \cdot (\mathrm{T_{cyl}} - \mathrm{T_{wall}}) \tag{6}$$

$$\dot{\mathrm{m}}_{\mathrm{evap}} = \mathrm{V_l} \cdot \Gamma_{\mathrm{g}} \tag{7}$$

$$\dot{\mathrm{U}}_{\mathrm{l}} = -\dot{U}_{\mathrm{evap}} - \dot{\mathrm{Q}}_{\mathrm{cyl}} \tag{8}$$

$$\dot{\mathrm{U}}_g = \dot{U}_{evap} - \mathrm{W} \tag{9}$$

where $\mathrm{m_p}$ is the total mass that needs to be accelerated, a the acceleration, D_{cyl} the diameter of the expansion chamber, p_{cyl} the working chamber pressure, p_{bp} the backpressure which is taken to be equal to atmospheric pressure. F_{fr} is the friction force based on the modified LuGre model of Tran and Yanada (2012), F_{load} the external load profile from the linear actuator, $\dot{\mathrm{Q}}_{\mathrm{cyl}}$ the thermal losses which are completely contributed to the liquid phase (Kanno and Shikazono, 2015), $\mathrm{h_{wall}}$ the heat transfer coefficient according to Woschni (1967), $\mathrm{A_{wall}}$ the perimeter of the working chamber, $\mathrm{T_{cyl}}$ the temperature of the working fluid, $\mathrm{T_{wall}}$ the temperature of the working chamber perimeter which is taken equal to the average of the start and end temperatures. $\dot{\mathrm{m}}_{\mathrm{evap}}$ is the evaporated mass, $\mathrm{V_l}$ the liquid volume, $\dot{\mathrm{U}}_{\mathrm{l}}$ and $\dot{\mathrm{U}}_g$ the change in internal energy of the corresponding phase, $\dot{U}_{evap}$ the transferred energy between the phases due to evaporation, and W the performed work which is attributed completely to the vapor phase (Kanno and Shikazono, 2015). The differential equations part of the friction model are also a part of the system that is solved, as well as the piston position which is the derivative of the piston velocity which is in part the derivative of the acceleration.

The variable set solved by the ODE system is sufficient to define the entire thermodynamic state with the extra assumptions of mechanical equilibrium and saturated vapor phase mentioned in section 1.2 together with the assumption that for small time steps the volume change of liquid is very small compared to the vapor volume change (Kanno and Shikazono, 2015). Only the liquid temperature has to be calculated separately as follows while other state variables can be determined based on the internal energy and density of each phase.

$$\mathrm{u}_l = \frac{U_l}{m_l} \tag{10}$$

$$\Delta \mathrm{T_{sup}} = \frac{u_l - u_{l,s}(p)}{c_{v,s}(p)} \tag{11}$$

$$\mathrm{T_l} = \mathrm{T_g} + \Delta \mathrm{T}_{sup} \tag{12}$$

where u_l is the mass specific internal energy of the liquid phase, $u_{l,s}(p)$ the mass specific internal energy of a saturated liquid at the current pressure, $c_{v,s}(p)$ the constant volume heat capacity for a saturated liquid at the current pressure, $\Delta \mathrm{T_{sup}}$ the liquid superheat, and $\mathrm{T_l}$ the metastable liquid temperature.

4. DESIGN RESULTS

The chosen refrigerant for the first dataset is HFO-R1233zd(E) because the critical pressure and temperature are above the range of interest and it is a low GWP refrigerant. It has also been shown to be a good candidate for low-temperature ORC applications and can be easily implemented as a replacement for R245fa (Datla and Brasz, 2014). The sizing model was used to simulate the expansion process for different initial states. An initial state is dependent on the saturation temperature and the vapor quality. All graphs presented here are simulations with an initial dead volume of 14.14 cm³, equivalent with a initial piston height of 20 mm and a piston diameter of 30 mm. The piston diameter was chosen based on possible expansion ratios while still confirming to production limitations and maximum linear actuator force. It should however still be large enough to accommodate all the measuring equipment. Figure 4 shows the displacement in function of the simulation time. Only the first second is shown because the piston position remains constant afterwards even though evaporation still takes place as will be presented later. For lower vapor qualities and

higher saturation temperatures the curves are steeper and higher expansion ratios are obtained. Another observation are the oscillations when the maximum volume is reached. This is due to the inertia of the mass in Equation (5).

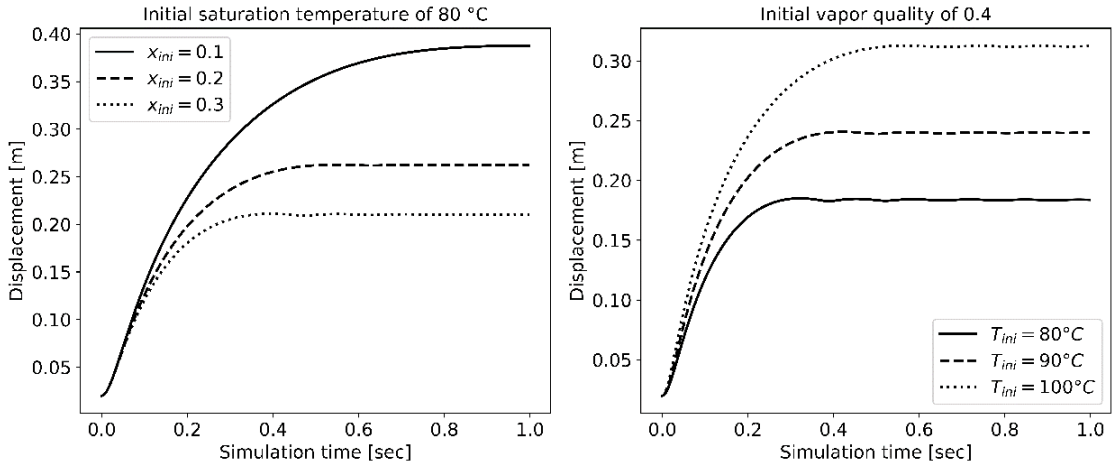

Figure 4: Displacement in function of simulation time for different initial conditions.

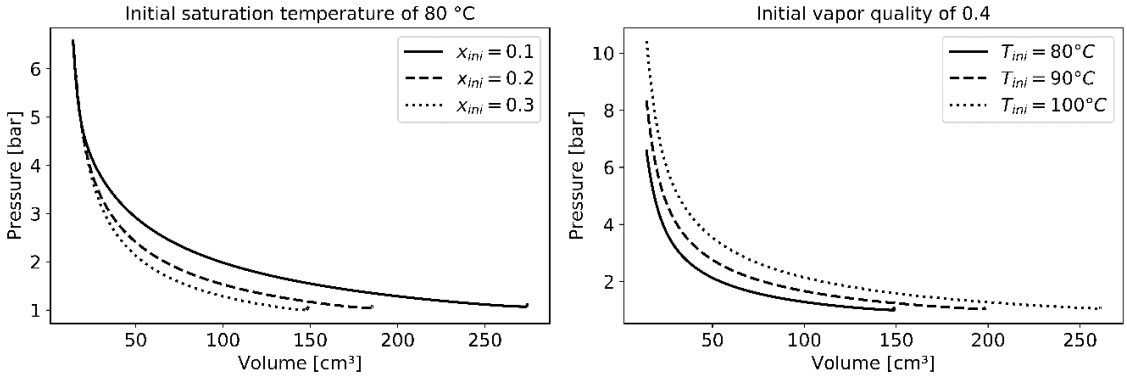

Figure 5: Simulated PV diagrams for different initial conditions.

Figure 5 shows the pressure in function of working chamber volume for different initial vapor qualities and for different initial saturation temperatures. These figures, together with Figure 4, clearly represent why a variable build-in volume ratio is important for a wide range of experimental data. This holds primarily true to be able to vary the initial vapor quality for the same expansion pressure ratio. This conclusion also highlights a difficulty in expander design for implementation in PEORC, where a small difference in inlet vapor quality represents a significant change in volumetric expansion.

The maximum required volume ratio can be found for the highest initial saturation temperature and the lowest vapor quality. Due to limitations on the production length of the test chamber, it will not be possible to compare the highest initial temperatures and lowest qualities with the lowest initial temperatures with the highest qualities for the same pressure ratio and dead volume, even for very small dead volumes. But both conditions can be compared to intermediate points. The maximum expected pressure inside the test chamber corresponds to the saturation pressure of the highest initial temperature that will be tested. For the first test chamber, this is a pressure of 10.4 bar corresponding to an inlet saturation temperature of 100 °C. This pressure induces a maximum Von Mises stress of 8 Mpa within the piston housing according to the equations of Lamé. This value includes a scaling factor of 3 to take into account the holes in the cylinder wall which have to be there for the measurement equipment. The piston housing material is chosen for its machinability, additionally the yield strength should be above the found value. The piston head material is chosen for its compatibility with the piston chamber material in the high frictional environment of a piston expander. The seal material should be compatible with the chosen working fluid and temperature range.

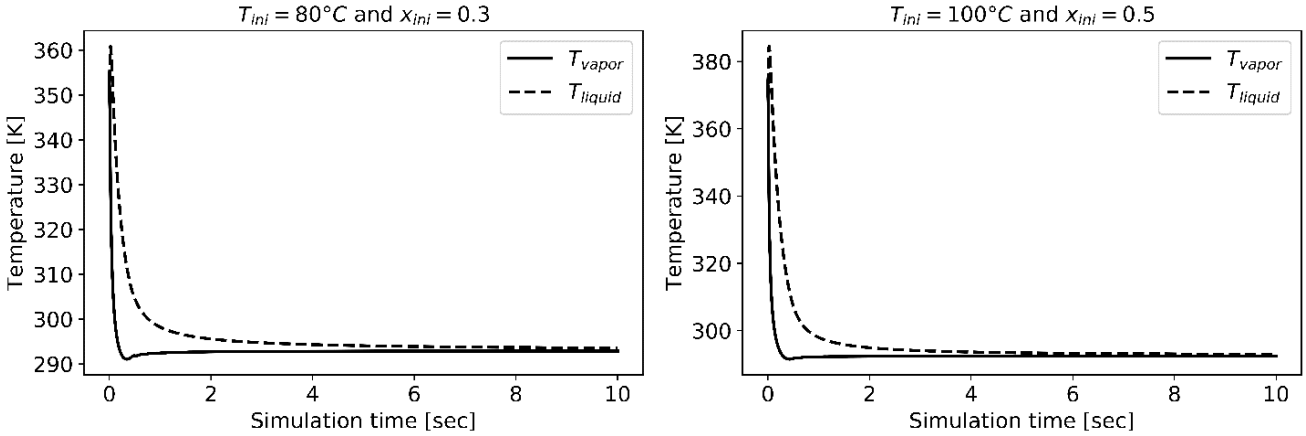

Figure 6: Vapor and liquid temperature in function of simulation time.

Another observation from Figure 5 is that the evaporation keeps occurring even after the complete expansion has finished. This is visible by the small increases in pressure at a constant maximum volume. The piston is thus no longer moving and the small pressure increase is due to final evaporation to equilibrium. These final stages of evaporation are no longer capable to overcome the static friction. This slow evaporation at the end of the simulation is also visible on Figure 6. Figure 6 shows the liquid and vapor temperatures in function of the simulation time for two initial conditions. The liquid superheat is a driving factor for evaporation, the bigger the liquid superheat the bigger the non-dimensional pressure difference (Equations 3 and 4) and the smaller the thermal relaxation time (Equation 2) which in turn implies greater vapor generation rates (Equation 1). However, the liquid superheat tends to 0 but never truly reaches it because it also lowers the evaporation rate. At a certain point a stopping requirement will be needed to evaporate completely to equilibrium. This requirement will be based on experimental observations.

The parameters of the first test chamber to be used are listed in Table 1. These are obtained from initial modeling of the expansion process with the implementation of the HRM while taking into account production limitations for parts.

Table 1: Nominal design values of the first test chamber.

Parameter	Value	Unit
Piston bore	30	mm
Maximum stroke	190	mm
Saturation temperature	80-100	°C
Saturation pressure	6.5-10.5	bar
Vapor quality	0-1	-
Working fluid	R1233zd(E)	-
Critical temperature	165.6	°C
Critical pressure	35.7	bar
GWP	~1	-
Molar mass	131	g/mol
Piston housing material	SS316L	-
Piston Head material	Messing	-
Seals material	PTFE	-

5. CONCLUSIONS

Currently, the majority of available heat sources are situated in the low-temperature range. Thermodynamic cycles that benefit from two-phase expansion show great potential. However, the impact of two-phase expansion on the design of these machines is hardly investigated. In this study, the design of a unique experimental test setup is elaborated that will be used the study the two-phase expansion phenomena within a reciprocating expander. Three

two-phase models are possible to use within simulations, taking into account the mechanical equilibrium and thermal non-equilibrium assumptions of volumetric expanders. The homogeneous relaxation model (HRM) is chosen in this work as it gives a straightforward but accurate framework to describe the flashing process from experimental data. Initial modelling shows that most of the superheated metastable liquid occurs until around 2 seconds after the start of expansion. The mechanical power will be provided by a linear actuator, making it possible to alter the build-in volume ratio and movement profile. The first experiments will consist of a piston with bore 30 mm and maximum stroke of 190 mm. The employed refrigerant will initially be R1233ZD(e) as a low GWP option in current low temperature ORC's. The tested saturation temperature range will be in the order of 80 to 100 °C in relation to these abundant low temperature sources. In future work these primary experiments will be used to empirically calibrate the parameters of the HRM model.

NOMENCLATURE

ϵ	void-fraction	(-)
ψ	pressure difference	(-)
ρ	density	(kg/m³)
Γ_g	vapor generation rate	(kg/m³s)
Θ	thermal relaxation time	(sec)
A	area	(m²)
a	acceleration	(m/s²)
c_v	constant volume heat capacity	(J/kgK)
D	diameter	(m)
F	force	(N)
h	heat transfer coefficient	(W/m²K)
m	mass	(kg)
p	pressure	(Pa)
Q	heat transfer	(J)
T	temperature	(K)
U	internal energy	(J)
u	mass specific internal energy	(J/kg)
V	volume	(m³)
W	work	(W)
x	vapor quality	(-)
$\bar{x}$	equilibrium vapor quality	(-)

Subscript

bp	backpressure
c	critical
cyl	cylinder
evap	evaporation
fr	friction
g	gas/vapor
l	liquid
p	piston
s	saturated
sup	superheat

Acronyms

BVR	Built in Volume Ratio
COP	Coefficient of Performance
GWP	Global Warming Potential
HRM	Homogeneous Relaxation Model
ORC	Organic Rankine Cycle
PEORC	Partial Evaporation Organic Rankine Cycle

PTFE	Polytetrafluoroethylene
SS	Stainless Steel
TLC	Trilateral Cycle

REFERENCES

Bailey, D., Callery, S., & Shaftel, H. (Eds.). (2022, February 23). *Climate change: Vital signs of the planet*. NASA. Retrieved March 1, 2022, from https://climate.nasa.gov/

Bianchi, G., Kennedy, S., Zaher, O., Tassou, S.A., Miller, J., & Jouhara, H. (2018). Numerical modeling of a two-phase twin-screw expander for Trilateral Flash Cycle applications. *International journal of refrigeration,* 88, 248-259.

Bilicki, Z., Kwidzinski, R., & mohammadein, S.A. (1996). Evaluation of the relaxation time of heat and mass exchange in the liquid-vapour bubble flow. *International journal of heat and mass transfer,* 39(4), 753-759.

Branchini, L., De Pascale, A., & Peretto, A. (2013). Systematic comparison of ORC configurations by means of comprehensive performance indexes. *Applied Thermal Engineering,* 61(2), 129-140.

Datla, B.V., & Brasz, J.J. (2014). Comparing R1233zd and R245fa for low temperature ORC applications. *Proceedings of the 15th international refrigeration and air conditioning conference.* (1-7). Purdue University.

Downar-Zapolski, P., Bilicki, Z., Bolle, L., & Franco, J. (1996). The non-equilibrium relaxation model for one-dimensional flashing liquid flow. *International journal of multiphase flow,* 22(3), 473-483.

Dumont, O., Dickes, R., & Lemort, V. (2017). Experimental investigation of four volumetric expanders. *Energy Procedia,* 129, 859-866.

Fischer, J. (2011). Comparison of trilateral cycles and organic Rankine cycles. *Energy,* 36(10), 6208-6219.

Forman, C., Muritala, I. K., Pardemann, R., & Meyer, B. (2016). Estimating the global waste heat potential. *Renewable and Sustainable Energy Reviews,* 57, 1568–1579.

Galoppi, G., Secchi, R., Ferrari, L., Ferrara, G., Karellas, S., & Fiaschi, D. (2017). Radial piston expander as a throttling valve in a heat pump: focus on the 2-phase expansion. *International journal of refrigeration,* 82, 273-282.

Imran, M., Usman, M., Park, B., & Lee, D. (2016). Volumetric expanders for low grade heat and waste heat recovery applications. *Renewable and Sustainable Energy Reviews,* 57, 1090-1109.

Kanno, H., & Shikazono, N. (2015). Experimental and modeling study on adiabatic two-phase expansion in a cylinder. *International journal of heat and mass transfer,* 86, 755-763.

Lecompte, S., van dan Broek, M., & De Paepe, M. (2013). Thermodynamic analysis of the partially evaporating trilateral cycle. *Proceedings of the 2nd international seminar on ORC power systems.* Rotterdam, Netherlands.

Lecompte, S., Huisseune, H., van dan Broek, M., Vanslanbrouch, B., & De Paepe, M. (2015a). Review of organic Rankine cycle (ORC) architectures for waste heat recovery. *Renewable and Sustainable Energy Reviews,* 47, 448-461.

Lecompte, S., van dan Broek, M., & De Paepe, M. (2015b). Performance potential of ORC architectures for waste heat recovery taking into account design and environmental constraints. In Editor, Lemort, V., Quoillin, S., De Paepe, M., & van den Broek, M. (Eds.), *Proceedings of the 3th international seminar on ORC power systems.(*1263-1273). Brussels, Belgium: University of Liège and Ghent University.

Lecompte, S., van den Broeck, M., & De Paepe, M. (2017). Initial design of an optical-access piston expansion chamber for wet-expansion. *Energy Procedia,* 129, 307-314.

Li, Z., Lu, Y., Huang, Y., Qian, G., Chen, F., Yu, X., & Roskilly, A. (2017). Comparison study of trilateral Rankine cycle, organic flash cycle and basic organic rankine cycle for low grade heat recovery. *Energy Procedia,* 142, 1441-1447.

Liao, Y., & Lucas, D. (2017). Computational modelling of flash boiling flows: a literature survey. *International journal of heat and mass transfer,* 111, 246-265.

Qyyum, M. A., Qadeer, K., Lee, S., & Lee, M. (2018). Innovative propane-nitrogen two-phase expander refrigeration cycle for energy-efficient and low-global warming potential LNG production. *Applied thermal engineering,* 139, 157-165.

Taniguchi, H., Kudo, K., Giedt, W.H., Park, I., & Kumazawa, S. (1988). Analytical and experimental investigation of two-phase flow screw expanders for power generation. *Journal of engineering for gas turbines and power,* 110(4), 628-635.

Tran, X.B., & Yanada, H. (2012). Modeling of dynamic friction behaviors of hydraulic cylinders. *Mechatronics*, 22(1), 65-75.

Vasuthevan, H., & Brümmer, A. (2016). Thermodynamic modeling of screw expander in a trilateral flash cycle. *Proceedings of the 23rd international compressor engineering conference.* (1-10). Purdue: Purdue University.

Wang, Q., Wu, W., He, Z., & Ziviani, D. (2019). Analysis of the intake process and its influence on the performance of a two-phase reciprocating expander. *Applied thermal engineering*, 160.

Woschni, G. (1967). A universally applicable equation for the instantaneous heat transfer coefficient in the internal combustion engine. *SAE technical papers*.

ACKNOWLEDGEMENT

I would like to thank the Research Foundation-Flanders for their financial support through FWO-Flanders grant (1SD9721N).